Strongly Coupled Fluid–Structure Interaction in a Three-Dimensional Model Combustor During Limit Cycle Oscillations

Mina Shahi
Faculty of Engineering Technology,
Laboratory of Thermal Engineering,
University of Twente,
Enschede 7500 AE, The Netherlands
e-mail: m.shahi@utwente.nl

Jim B. W. Kok
Faculty of Engineering Technology,
Laboratory of Thermal Engineering,
University of Twente,
Enschede 7500 AE, The Netherlands

J. C. Roman Casado
Faculty of Engineering Technology,
Laboratory of Thermal Engineering,
University of Twente,
Enschede 7500 AE, The Netherlands

Artur K. Pozarlik
Faculty of Engineering Technology,
Laboratory of Thermal Engineering,
University of Twente,
Enschede 7500 AE, The Netherlands

Due to the high temperature of the flue gas flowing at high velocity and pressure, the wall cooling is extremely important for the liner of a gas turbine engine combustor. The liner material is heat-resistant steel with relatively low heat conductivity. To accommodate outside wall forced air cooling, the liner is designed to be thin, which unfortunately facilitates the possibility of high-amplitude wall vibrations (and failure due to fatigue) in case of pressure fluctuations in the combustor. The latter may occur due to a possible occurrence of a feedback loop between the aerodynamics, the combustion, the acoustics, and the structural vibrations. The structural vibrations act as a source of acoustic emitting the acoustic waves to the confined fluid. This leads to amplification in the acoustic filed and hence the magnitude of instability in the system. The aim of this paper is to explore the mechanism of fluid–structure interaction (FSI) on the LIMOUSINE setup which leads to limit cycle of pressure oscillations (LCO). Computational fluid dynamics (CFD) analysis using a RANS approach is performed to obtain the thermal and mechanical loading of the combustor liner, and finite element model (FEM) renders the temperature, stress distribution, and deformation in the liner. Results are compared to other numerical approaches like zero-way interaction and conjugated heat transfer model (CHT). To recognize the advantage/disadvantage of each method, validation is made with the available measured data for the pressure and vibration signals, showing that the thermoacoustic instabilities are well predicted using the CHT and two-way coupled approaches, while the zero-way interaction model prediction gives the largest discrepancy from experimental results. [DOI: 10.1115/1.4038234]

Keywords: fluid–structure interaction, pressure oscillation, 3D combustor, thermoacoustic instability

1 Introduction

A well-known problem of lean premixed combustion of natural gas in gas turbine combustors is the sensitivity to thermoacoustic instability [1,2]. These combustors can spontaneously exhibit significant flow and pressure oscillations. These oscillations may reach such high amplitudes that they cause flame extinction, structural vibration, flame flashback, and ultimately failure of the system [3,4]. Several coupled mechanisms are known to promote such interactions, for example, flame–acoustic wave interactions [5], flame vortex interactions [6], thermal–structure interactions [7,8], and fluid–structure interactions (FSI) [9,10], and all of them may be present in a system individually or simultaneously [11,12]. The liner of a gas turbine combustor is a flexible structure that is exposed to the pressure oscillations occurring inside the combustor. These pressure oscillations can be of very high amplitude due to the thermoacoustic instability, i.e., when the fluctuations of the rate of heat release and the acoustic pressure waves amplify each other. The liner structure is a dynamic mechanical system that vibrates at its own eigenfrequencies and at the frequencies by which it is forced by the exposed pressure oscillations. On the other hand, the liner vibrations force a displacement of the flue gas near the wall in the combustor. The displacement is very small, but it may act like a distributed acoustic source which is proportional to the liner wall acceleration. Hence, the liner and combustor are a coupled elasto-acoustic system. When this is exposed to the limit cycle of pressure oscillations (LCO), the liner may ultimately fail due to fatigue. Modeling the interaction between the fluid and structure in a combustion system allows us to predict the effect of vibrating walls on the flame dynamics and also recognize the hazard frequencies at which thermoacoustic instabilities may occur. The feedback mechanism of thermoacoustic instabilities has attracted much attention in the past decade and has been extensively reviewed [1,13,14]. Coupled fluid–solid interaction phenomena, which are characterized by the interaction of the fluid forces and structural deformations, appear in many applications on different fields of science and engineering [15–17]. However, research on the issues related to interaction between the combustion processes and the structure during the LCO is very limited. Developing efficient and accurate solvers to model complex fluid–structure interaction problems for this application is still a challenging task. Here, contrary to, for example, air plane wing structural vibration, the vibrations of a gas turbine combustor liner are high in frequency and small in amplitude. This combination of characteristics is, however, very dangerous with a view to high cycle fatigue.

Huls et al. [9] reported measurements and calculations carried out on a 500 kW test rig. They calculated the excitation pressure on the structure by using large eddy simulation and used the calculated pressure field as a load in a finite element model (FEM) to measure the wall vibrations. In their approach, only one-way coupling was considered with the structure, and indeed no

Contributed by the Combustion and Fuels Committee of ASME for publication in the Journal of Engineering for Gas Turbines and Power. Manuscript received February 8, 2017; final manuscript received July 21, 2017; published online January 30, 2018. Editor: David Wisler.

information from the structural domain was fed back into the large eddy simulation. Later, Pozarlik [18] performed FSI numerical simulations with application on the same test rig with both one- and two-way approaches using a weak coupling method. However, this work was limited to a stable combustion condition, as the combustor could not be operated in the LCO regime. A similar analysis was done by Alemela et al. [19] on a bluff body flame stabilized combustor (the same test rig as is under the study in this paper), considering a two-dimensional slice instead of the full geometry. Nevertheless, the study was done using the two-way coupling, and during the LCO condition, the work did not explore the effect of the combustion model and modeling approach. Additionally, at the time validation data for the predicted displacement were not available, yet. Altunlu et al. [20] performed the coupled FSI simulation on the same combustor. They extended the model to full three-dimensional (3D), modeling half of the combustor instead of a two-dimensional slice to include the 3D flow patterns and to take into account the structural system stiffness due to the rectangularly connected geometry of the four walls. However, their model failed in the prediction of the unstable combustion due to the assumed symmetry condition in the middle plane. The study presented in the current paper shows that the mentioned assumption pushes the flame to the stable regime. In this paper, two-way fluid–structure interaction is studied for turbulent partially premixed methane air combustion. The method employed is the partitioned simulation of the coupled system composed of the liner and the flue gas domain; both the method and the results will be presented. Despite the one-way interaction method which allows sending information only from the computational fluid dynamics (CFD) code to the computational structure dynamics code, the two-way coupling method gives the possibility for the full exchange of data between fluid and solid solvers. This work is done in the framework of the LIMOUSINE project. The investigated combustor resembles the industrial gas turbine combustors by: a flame stabilized by a recirculation area, a narrow burner flow passage, an upstream cold flow area, and an acoustically closed air inlet [21]. Therefore, it is expected that the limit cycle phenomenon under study is relevant to the situation of a gas turbine combustor, and the methodology and generated data are of interest for the subsequent investigation of flame characteristics.

2 Thermo-acoustic

Thermo-acoustic instability is a phenomenon in which pressure and heat release interact with each other in a confined domain. The relation between a flame and the acoustic field was studied by Rayleigh [22]. The Rayleigh criterion characterizes the thermoacoustic system to be damped or to have amplified interaction between pressure and heat release. It states that if pressure and heat release fluctuations are in phase, the instabilities are enhanced, whereas the instabilities are damped when the pressure oscillations and heat release are out of phase. This criterion is expressed in the following equation:

$$\int\int_V\int p'q'dV > 0 \tag{1}$$

where p' and q' are pressure and heat release fluctuations, respectively, integrated over one cycle of the oscillation and V is the flow domain. Note that the integrals are also spatial, which means that both effects, destabilizing and stabilizing, can occur in different locations of the combustor and at different times, so the stability of the combustor will be decided by the net mechanical energy added to the combustor domain. Indeed, when the acoustic energy losses match the energy gain, a stationary oscillatory behavior is obtained, which is referred to as the limit cycle oscillation.

However, Rayleigh's criterion is a necessary but not a sufficient condition for the instabilities to occur [23,24]. Therefore, Eq. (1) has been extended to Eq. (2) to include the losses of acoustic energy at the boundaries and entropy effects. According to Eq. (2), the acoustic energy growth rate depends not only on the Rayleigh term but also on the acoustic fluxes; therefore, the Rayleigh criterion is only a necessary condition for instability to occur

$$\int_V\int_T p'(x,t)Q'(x,t)\,\mathrm{d}t\,\mathrm{dV} - \frac{\gamma\overline{p}}{\gamma-1}\int_A\int_T p'(x,t)u'(x,t)\,\mathrm{d}t\,\mathrm{dA} > 0 \tag{2}$$

3 Combustor Setup Description

The test case, which is modeled in the work presented here, is based on a test rig developed within the framework of the European LIMOUSINE project (see Fig. 1 for details). The setup is designed specifically to study limit cycles due to thermo-acoustic instability. The combustion chamber consists of two rectangular ducts with different widths. The upstream duct has a $25 \times 150\,\mathrm{mm}^2$ cross section and is 275 mm long, whereas the downstream duct has a $50 \times 150\,\mathrm{mm}^2$ cross-sectional area to compensate the volume expansion due to the combustion. In the transition between the ducts, a wedge is mounted that stabilizes the flame. The total length of the combustor is 1050 mm. This configuration behaves like a variation of a Rijke tube [25]. It deviates from the standard Rijke tube because it is acoustically closed at the upstream end and opens to the atmosphere at the downstream end. Air, as the oxidizer, is injected by means of two choked nozzles at the upstream end. The flow recirculation that stabilizes the flame is created by a wedge, which is placed at the point where the small duct is attached to the large duct. The gaseous fuel is injected through 62 holes fed by choked nozzles at either end of the wedge (see Fig. 1(*c*)). The fuel used here is methane at room temperature. All pieces of the test rig, except the brass wedge shaped bluff body, are made from heat-resistant stainless steel S310. The only cooling of the combustor is by natural convection and radiation at the outside surfaces. The burner can operate at a range of power of 20–80 kW and air factor 0.8–2.

4 Fluid–Structure Interaction Approach

In order to reduce time and cost in such multiphysics problems, the methods used for numerical simulation of coupled systems become more and more important [26]. In general, the approaches to the field of coupled problems can be divided into two classes: one being called monolithic [27,28] and the other partitioned [29–31]. Monolithic or so-called simultaneous procedure solves the coupled system in a single iteration loop with consistent time integration schemes for all physical fields using one single computer code; this leads to time accurate coupled solutions, and larger time steps can be used as compared to partitioned schemes for the same level of accuracy [32]. However, it is still computationally more expensive per time-step compared to the partitioned approach. In this work, the latter approach for the fluid–structure interaction is used. The partitioned method is an approach in which the two separate solvers with the appropriate interface boundary conditions for the flow domain and the structural domain operate in a coupled way [33]. A time lag in the integration of the fluid and structure domains is the main drawback of this approach. However, the principal advantage is application of the existing sophisticated solvers for each subsystem. The partitioned approach strives to solve each physical field separately with communication of interface data in between to connect the components. Interface conditions are enforced asynchronously, meaning that the flow of the fluid does not change while the structural equations is being solved and vice versa. The total mesh displacement is transferred across the interface by preserving the profile between the two fields, while the total force will be transferred using a conservative formulation (see more details in Ref. [18]). Thus, at the interface between fluid and solid regions the matching conditions should satisfy the Euler equation and Cauchy stress, as

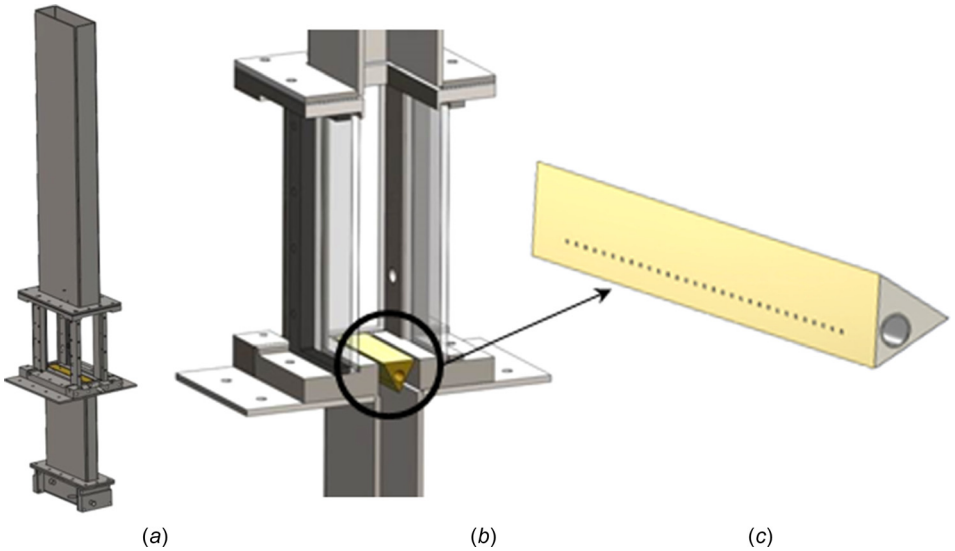

Fig. 1 (*a*) LIMOUSINE test rig, (*b*) optical access section, and (*c*) triangular bluff body with injection holes

$$\rho_f \cdot \mathbf{n} \cdot \ddot{\mathbf{u}} = -\nabla p \cdot \mathbf{n}$$
$$\mathbf{t} = -p \cdot \mathbf{n} \tag{3}$$

where p is the pressure, ρ_f the fluid density, $\mathbf{n}$ is the normal direction vector, $\mathbf{t}$ is the Chauchy stress vector in the solid, and $\mathbf{u}$ is the displacement vector.

In view of the strength of preserving the overall system stability, the partitioned method can be categorized into weak and strong coupling schemes [34,35], which are also named, respectively, as explicit and implicit [35]. The interface iterations of the strong coupling scheme can be computationally very expensive, especially for the fluid part of the FSI simulation which has many unknowns. However, in case of a highly flexible structure, weak coupling introduces a major error and might even lead to failure of the entire simulation [36]. Here, due to the complexity of the problem under study, the partitioned approach is used. Since the liner of the combustor has a small thickness, it can be very flexible, and hence, the weak coupling scheme might not be an appropriate approach. Therefore, the strong coupling is selected. The schematic view of two-way fluid–structure interaction numerical simulation conducted in this paper is shown in Fig. 2. During the two-way interaction analysis, the CFX and ANSYS MECHANICAL software exchange information dynamically every time-step. The data from a steady-state solution are fed into the static structural analysis and then to the transient structural and fluid flow. A two-way coupling between the fluid and structure is obtained by linking the transient modules and then transferring surface loads/displacements across the interface. The quantities from the fluid computations are applied directly on the liner, and then the new

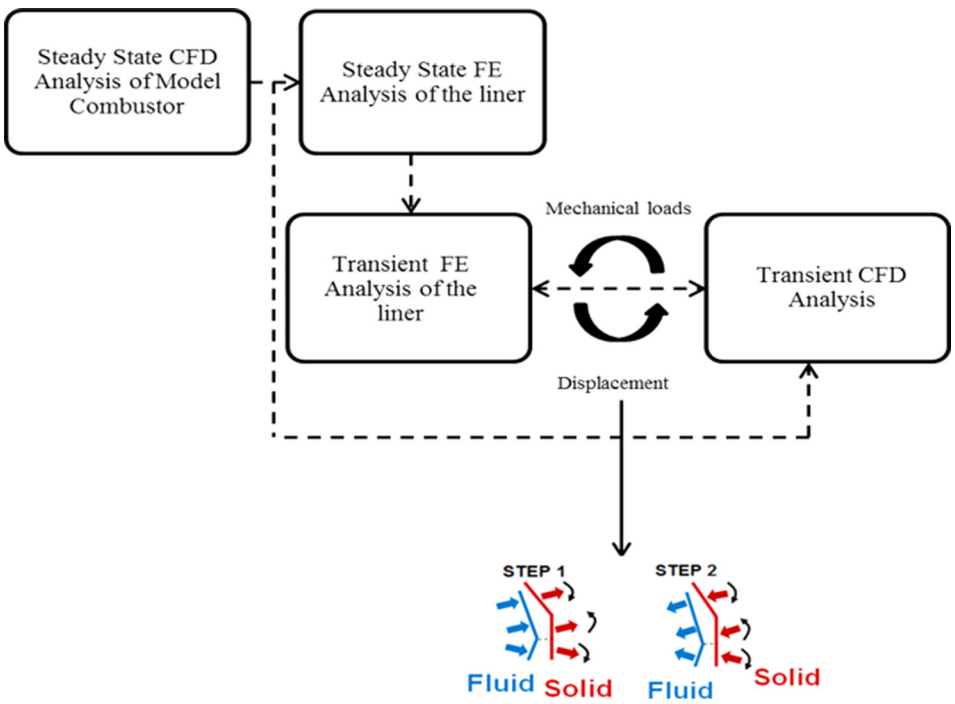

Fig. 2 Schematic representation of FSI approach

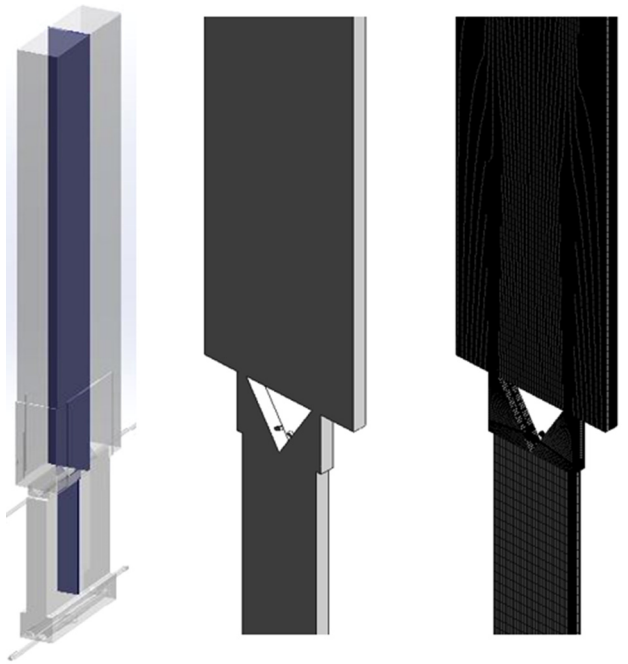

Fig. 3 (*a*) CFD domain: 4 mm slice of the total geometry, (*b*) enlarged view around the burner, and (*c*) mesh details of the LIMOUSINE combustor: enlarged view around the flame holder

deformed structure is updated in the fluid simulation. This procedure will be repeated until a converged solution is obtained. Calculations will then continue in the next time-step (Fig. 2).

4.1 Computational Fluid Dynamics Numerical Simulation. In order to reduce the computational effort, numerical calculations of the reacting flow inside the chamber are done only for a thin slice of the combustor (see Fig. 3). The spanwise size of the numerical domain is 4 mm wide with symmetry conditions enforced on each side. The choice of the CFD domain and hence the boundary conditions is important for estimating the magnitude of the instability, as it can add an artificial damping to the system by restricting the three-dimensional turbulent motion of the reacting flow. Since the resolution of the grid has significant effects on the accuracy of results, several different meshes with various element sizes and distributions were tested for steady case, and finally, a total number of 644,000 elements are used for the mesh. All the meshes used in this study are generated using the meshing tool ANSYS WORKBENCH 14.5. The impact of the meshing technology and sensitivity of the results on the grid have been studied by Shahi et al. [37] focusing on the fluid-only simulation. The mesh is refined in the combustion zone and around the fuel inlets.

The CFD code employed here is ANSYS CFX 14.5. It uses an implicit finite volume formulation to construct the discretized equations representing the Reynolds-averaged Navier–Stokes equations for the fluid flow. The model consists of a compressible solver with a co-located finite volume method, such that the control volumes are identical for all transport equations [38]. The

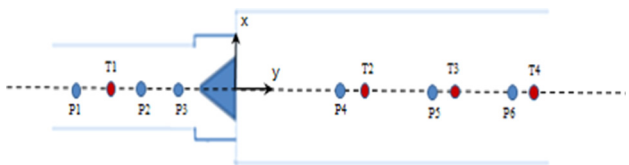

Fig. 4 Pressure and temperature monitoring points in the CFD domain

basic set of balance equations solved by ANSYS CFX comprises the continuity, momentum, species, and energy transport equations. The instantaneous balance equations for the fluid domain can be written with the application of Favre averaging and in Cartesian coordinates as follows:

— Conservation of mass

$$\frac{\partial \overline{\rho}}{\partial t} + \frac{\partial (\overline{\rho}\widetilde{u}_i)}{\partial x_i} = 0 \tag{4}$$

— Momentum

$$\frac{\partial (\overline{\rho}\widetilde{u}_i)}{\partial t} + \frac{\partial (\overline{\rho}\widetilde{u}_i\widetilde{u}_j)}{\partial x_i} = -\frac{\partial \overline{p}}{\partial x_i} + \frac{\partial}{\partial x_i}\left(\overline{\tau_{ij}} - \overline{\rho u_i'' u_j''}\right) \tag{5}$$

$\boldsymbol{\tau}$ is the stress tensor which is related to the strain rate by

$$\overline{\tau_{ij}} = \widetilde{\tau_{ij}} + \overline{\tau_{ij}''} \tag{6}$$

— Chemical species

$$\frac{\partial (\overline{\rho}\widetilde{Y}_k)}{\partial t} + \frac{\partial (\overline{\rho}\widetilde{Y}_k\widetilde{u}_i)}{\partial x_i} = -\frac{\partial \left(\overline{\rho}\widetilde{u_i'' Y_k''}\right)}{\partial x_i} - \frac{\partial (\overline{V_{k,l}Y_k})}{\partial x_i} + \overline{\dot{\omega}}_k \tag{7}$$

— Energy equation

$$\frac{\partial (\overline{\rho}\widetilde{e_0})}{\partial t} + \frac{\partial}{\partial x_j}\left(\overline{\rho}\widetilde{u}_i\widetilde{e_0} + \widetilde{u}_j\overline{p} + \overline{u_j'' p} + \overline{\rho u_j'' e_0''} + \overline{q_j} - \overline{u_i \tau_{ij}}\right) = 0 \tag{8}$$

which $\widetilde{e_0}$ is given by

$$\widetilde{e_0} \equiv \widetilde{e} + \widetilde{u}_k\widetilde{u}_k/2 + k \tag{9}$$

where the turbulent energy, k, is defined by

$$k = \frac{u_k'' u_k''}{2} \tag{10}$$

For the discretization of the governing equations, a high-resolution advection scheme spatial method and a second-order backward Euler discretization for time accuracy is used to solve the unsteady RANS equations. The unclosed terms contain products of fluctuating values, i.e., $\overline{\rho u_i'' u_j''}$ and $\overline{\rho}\widetilde{u_i'' Y_k''}$ which need to be closed by modeled terms. In this work, the effects of turbulence are described by using the shear stress transport turbulence model in the steady-state calculations, while for the transient calculations the scale-adaptive simulation model is used. The choice of turbulence model greatly influences the prediction of turbulent mixing rate and hence limits cycle oscillations. A comparison between the standard k–ω and shear stress transport-scale-adaptive simulation model for the similar combustor has been reported earlier by Kumar et al. [39]. Reacting flow simulations are carried out on the model combustor by using the burning velocity model using a new model option for improving accuracy for nonpremixed flames [40]. Burning velocity model uses a RIF flamelet library for the "burnt" mixture. This mechanism involves 16 species and 46 reversible reactions scheme for methane–air gas chemistry [41].

Table 1 Operating condition

Power (kW)	Air factor	Methane mass flow rate (g/s)	Air mass flow rate (g/s)
40	1.4	0.8	19.152

The flow parameters are set consistent with the experimental conditions depicted in Table 1. Unsteady RANS simulations are carried out with a time-step of 1×10^{-5} s. The convergence criterion of the RMS normalized residual values is set to 1×10^{-5}. Pressure fluctuations and temperature changes are monitored at locations shown in Fig. 4.

4.1.1 Mesh Deformation. In order to account for the mesh movement, it is necessary to modify the governing equations to include the mesh deformation. The transient convection term must change as the control volumes deform in time. These modifications follow from the application of the Leibnitz rule:

$$\frac{\mathrm{d}}{\mathrm{d}t}\int_{V(t)} \varphi dV = \int_V \frac{\partial \varphi}{\partial t} dV + \int_s \varphi W_j dn_j \tag{11}$$

where W_j is the velocity of the control volume boundary.

The differential conservation equations are integrated over a given control volume. At this juncture, the Leibnitz rule is applied, and the integral conservation equations become

$$\frac{\mathrm{d}}{\mathrm{d}t}\int_{V(t)} \rho dV + \int_s \rho(U_j - W_j) dn_j = 0 \tag{12}$$

$$\frac{\mathrm{d}}{\mathrm{d}t}\int_{V(t)} \rho U_j dV + \int_s \rho(U_j - W_j) U_j dn_j = -\int_s P dn_j + \int_s \mu_{\mathrm{eff}} \left(\frac{\partial U_i}{\partial x_j} + \frac{\partial U_j}{\partial x_i}\right) dn_j + \int_V S_{U_i} dV \tag{13}$$

V is the volume, S is the surface, and μ_{eff} is the effective viscosity including the dynamic viscosity and the turbulent viscosity

$$\frac{\mathrm{d}}{\mathrm{d}t}\int_{V(t)} \rho\varphi dV + \int_s \rho(U_j - W_j)\varphi dn_j = \int_s \Gamma_{\mathrm{eff}} \left(\frac{\partial \varphi}{\partial x_j}\right) dn_j + \int_V S_\varphi dV \tag{14}$$

The transient term accounts for the rate of change of storage in the deforming control volume, and the advection term accounts for the net advective transport across the control volume's moving boundaries. The mesh deformation given by Eq. (14) is only attributed to the motion of nodes on the boundary. The motion of all remaining nodes (i.e., the regions of nodes with the same degrees-of-freedom) is determined with the displacement diffusion model. With this model, the displacement of domain boundaries is diffused to other mesh points by solving the following equation:

$$\nabla \cdot (\Gamma_{\mathrm{dis}} \nabla \delta) = 0 \tag{15}$$

In this equation, δ is the displacement relative to previous mesh locations and Γ_{dis} is the mesh stiffness, which determines the degree to which regions of nodes move together. It is worth noting that the displacement diffusion model for mesh motion is designed to preserve the relative mesh distribution of the initial mesh (more details are given in Ref. [42]).

4.2 Computational Structure Dynamics Computation. The finite element solver is used for the calculation of the structural domain. Because most of the dynamic coupling between the fluid and structure occurs in the region downstream of the wedge where the reaction takes place, only the structure downstream of the wedge is considered. To reduce the necessary computational efforts, the solid domain has been simplified, i.e., quartz glass windows or holes for thermocouples and pressure transducers have been removed. In order to determine the structural eigenfrequencies and mode shapes, modal analysis is first performed using the element type solid 186. Since the liner is clamped at the burner inlet plane, the air/fuel duct (i.e., plenum) is removed from the structural domain. The mode shape and eigenfrequencies of the first seven modes of the structure are presented, respectively, in Fig. 5 and Table 2. Compared to the measurements performed by Altunlu [43], the predicted eigenfrequencies are acceptable except for the first torsional and the second bending mode in which 18% deviation can be observed. The deviation between the measurements and prediction can be caused by the effect of welds in the structure which is neglected in the FEM [3]. It can be also attributed to other simplifications made in the model such as neglecting the effect of thermocouples and pressure transducers. Besides, in the FEM the plenum is removed and only the top liner is considered. Overall, frequencies predicted by the model using solid elements are close to the experimental data. However, considering that the plate modes of the structure are the only modes influencing the acoustic response of the combustor to the flame due to the associated change in the acoustic volume, the chosen FE model is claimed to be in line with the physical model. It is important to mention that both the measurements and calculations have been performed for the room temperature condition, as it is not possible to do such measurements in high temperature with the available tools in the laboratory. Therefore, a reduction in the represented eigenfrequencies is expected, as Young's modulus (E) is decreased for higher values of temperature. The structural eigenfrequency is indeed proportional to the square root of Young's

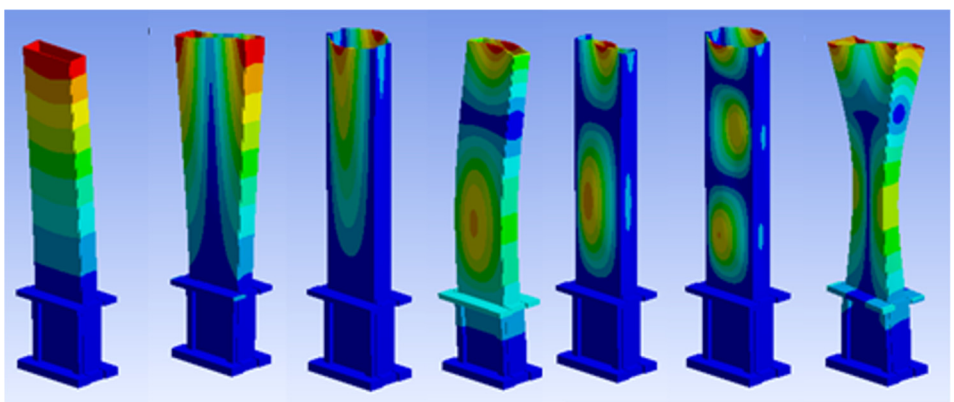

Fig. 5 Mode shape of the combustor (without the plenum) predicted by FEM

Table 2 Structural eigenfrequencies of the LIMOUSINE combustor at room temperature

	Structure eigenfrequencies	
Mode	Hammer test [1]	FEM solid elements
Bending (first)	125	126
Torsional (first)	534	437
Plate (first)	639	633
Bending (second)	645	532
Plate (second)	673	671
Plate (third)	744	750
Torsional (second)	764	761

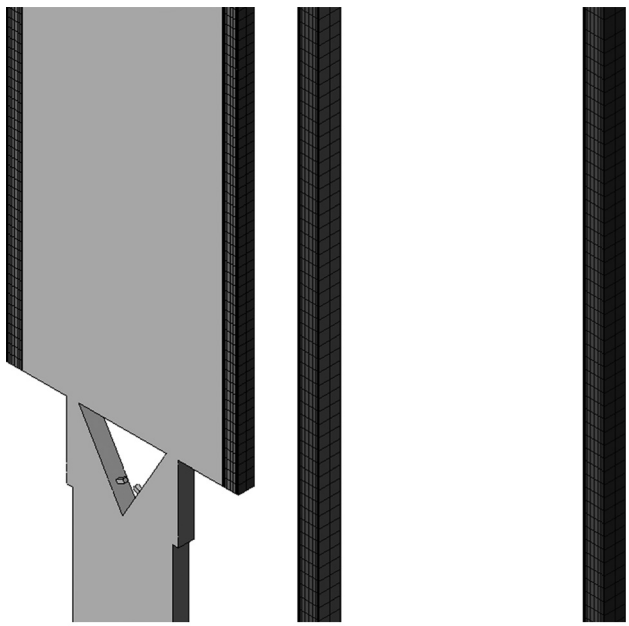

(*a*) (*b*)

Fig. 6 (*a*) Reduced structure domain attached to the fluid and (*b*) sketch of the solid mesh in the FE solver

modulus [44]. As Young's modulus reduces from 198 GPa to 176 GPa, an approximate reduction of 7% in the predicted eigenfrequencies is expected in the assumed hot condition (i.e., 400 °C). Further increase in the structure temperature leads to the further reduction in the predicted eigenfrequencies. Despite all simplifications of the studied geometry made in the FE model, the domain for the coupled simulation is still computationally very expensive when used for FSI. Therefore, only a slice of the structure is used for the further calculations. The chosen solid domain is sketched in Fig. 6. The structural mesh consists of 3304 elements of type solid 185 [45]. The linear elements have eight nodes with three degrees-of-freedom at each node. For simplification, a uniform temperature of 400 °C is assumed along the liner wall, and the material properties are determined as presented in Table 3. The clamped boundary condition is implemented at the burner inlet plane, while the rest of the surface is allowed to deform freely depending on the dynamic pressure loads.

Table 3 Material properties of SS310 at 400 °C

Young's modulus (GPa)	Poisson's ratio	Density (kg/m^3)
1.76	0.3	7715

5 Results

Results are compared with the other approaches like zero-way interaction so-called fluid-only model and also the thermal coupling approach of fluid and structure (conjugated heat transfer (CHT)). Details about these models can be found in previous work done by Shahi et al. [37,46] and Filosa et al. [47], where investigation of the sensitivity and accuracy of the reactive flow field prediction is conducted with regard to choices in computational mesh and turbulent combustion model. In this section, numerical results are presented and validated with available experimental data. However, prior to the discussion on the predicted multiphysics data, it is necessary to assure that the strong coupling is achieved by having the converged loads passing between two solvers. Here, minimum values of 1 and maximum values of 10 were selected for the staggered iteration; however, during the calculations always less than 10 loops were required, proving that the convergences occur before reaching to the upper limit. The convergence level of the force (**F**x, **F**y) and displacement (**U**x, **U**y) which are presented in Fig. 7 show that each quantity is converged as the residual drops below zero [42].

5.1 Acoustic Behavior. The geometric enclosure of the combustor may act as a resonator. Pressure waves which are reflected at the boundaries of the burner may interact with the heat release process. If the dissipation of acoustic energy within the chamber and also at the boundaries is smaller than the energy gained by the acoustic disturbances, pressure waves are excited and pressure amplitudes will soon grow up to a saturation limit. Figure 8 shows

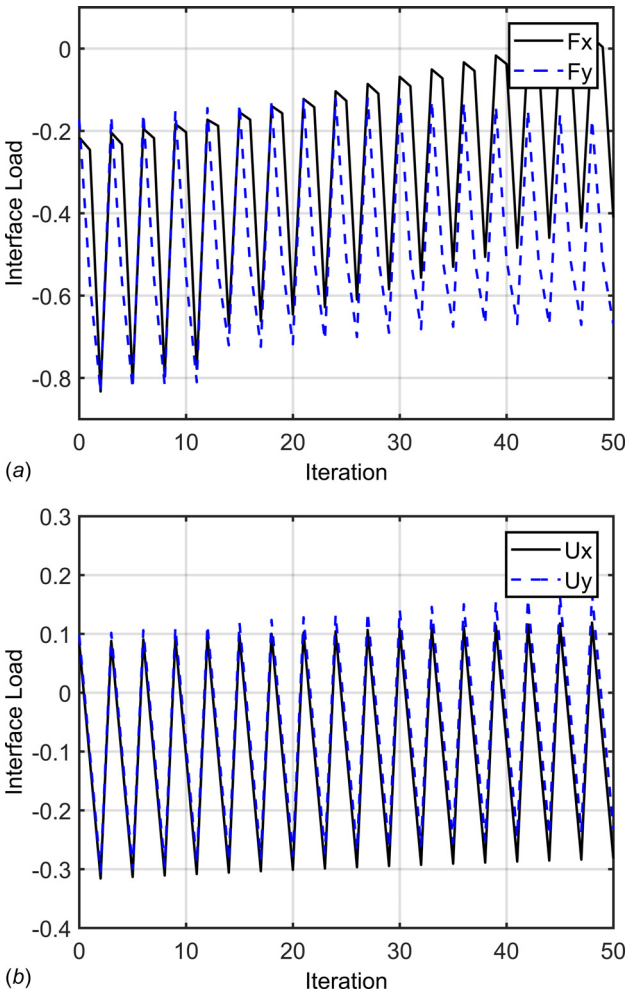

Fig. 7 Convergence of the interface loads: (*a*) mechanical load (LHS) and (*b*) wall displacement (RHS)

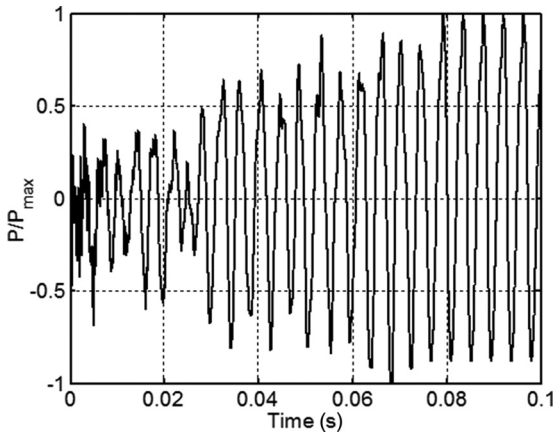

Fig. 8 Calculated self-exited pressure oscillation as a function of time

the calculated evolution of pressure over time within the burner recorded by the first control point above the wedge, which corresponds to the physical location of the first pressure transducer in the experiment. Due to the rapid growth of the oscillation amplitude characterizing the phase of oscillation, the system will soon reach to saturated constant amplitude.

The frequency spectrum of the pressure signal corresponding to the thermal power of 40 kW and $\lambda = 1.4$ using three different numerical approaches (fluid-only, CHT and two-way) together with the experimental measurements are plotted in Fig. 9. Both CHT approach and two-way coupled model predict the primary instability at 232 Hz giving the error of 0.6%; however, the numerical results based on the two-way approach show an overprediction of the instability magnitude inside the combustion chamber, giving 5% discrepancy from experimental results. This is mainly due to the overprediction of the temperature in the CFD domain in the two-way coupled approach compared to the CHT model, as a constant temperature has been set at the structure. It results in the underprediction of the heat losses through the combustion chamber, which is shown in Fig. 10. The area integral of the heat flux over the liner of the combustor in each case shows the clear difference between the two-way FSI approach and the CHT model. Considering that the observed difference in the predicted heat loss is just attributed to a 4 mm slice of the total depth of the combustor, the importance of this diversity will be even more significant. Among the used models, the zero-way interaction model shows the largest discrepancy from experimental results (an error about 10%) in the prediction of instability frequencies. However, the pressure spectrum presented in Fig. 9 shows the fundamental quarter wave mode frequency for each approach. According to the calculations, the first and third amplitude peaks are observed at frequencies presenting the first and the third quarter wave modes, with the part downstream the bluff body driving the instability process; this means that the instabilities are originating from the combustion chamber and not the whole combustor. Another observed peak is exactly double of the first eigenfrequency of the combustor. According to Roman Casado [48], this second peak appears due to the frequency doubling of the first eigenfrequency, which is mainly due to the presence of high nonlinearities in the combustion process when a system reaches high-amplitude limit cycle oscillations. This frequency indeed is driven by the first eigenmode. The measured pressure field shows a strong harmonic component near 600 Hz (period 1.67 ms), which is related to the structural dynamics of the combustion chamber. While in the two-way approach, the presence of structural dynamics is rather in the frequency range of 700–800 Hz. This can be due to the higher stiffness compared to the experiments caused by the assumed uniform temperature and therefore constant Young's modulus in the simulations. Table 4

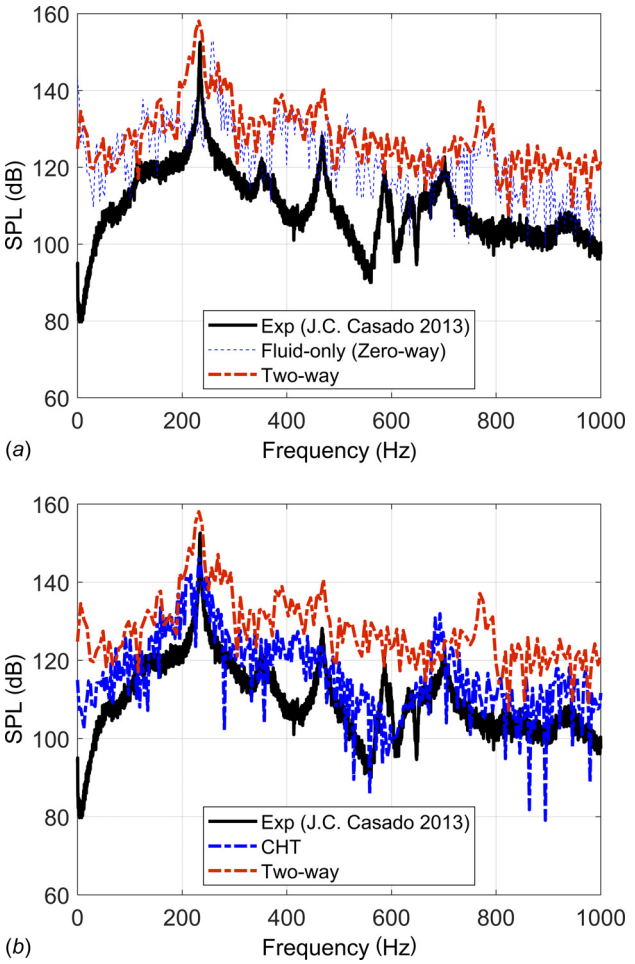

Fig. 9 Pressure spectrum for 40 kW and $\lambda = 1.4$: (*a*) experiment, zero-way and two-way interaction and (*b*) experiment, CHT, and two-way interaction

reports CFD, FEM, and experimental resonant frequencies, showing a good level of agreement. Furthermore, the FEM results show that the main frequency of instability is related to acoustics of combustion chamber and not the full geometry. To explore the origin of instability observed in Fig. 9, further analyze is conducted. As reported by Sivakumar and Chakravarthy [49] for a bluff body combustor, variation of dimensionless quantities such as the Helmholtz and Strouhal numbers with the Reynolds number

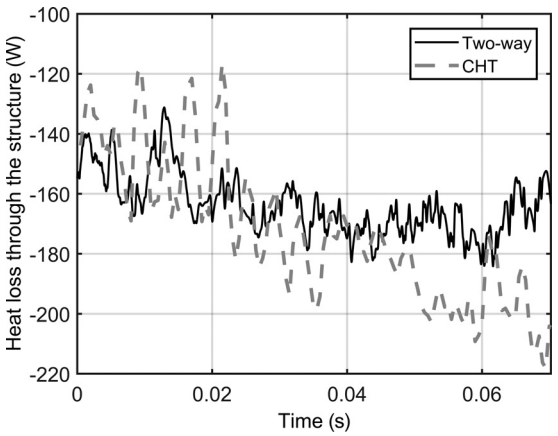

Fig. 10 Total calculated heat loss through the structured (i.e., 4 mm slice)

Table 4 Experimental, CFD, and analytical frequencies of first predicted peak frequency

		Resonance frequency (Hz)				
Power (kW)	λ	Experiment Ref. [3]	CFD fluid-only (zero-way)	CFD (CHT)	CFD (FSI)	FEM combustion chamber/no mean flow
40	1.4	234	256	232	232	249

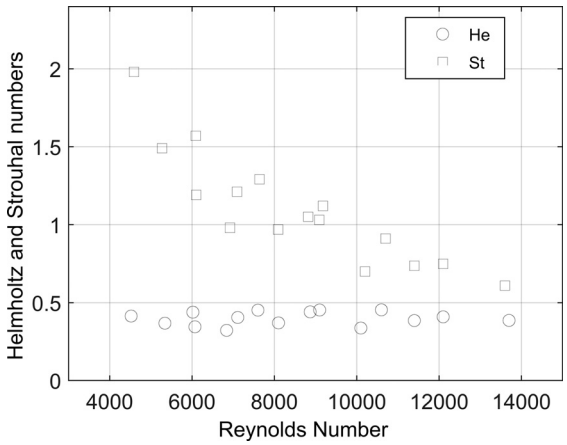

Fig. 11 Variation of the measured Helmholtz number (He) and Strouhal number (St) with the Reynolds

can determine the origin of the LCO. The Helmholtz and Strouhal numbers are, respectively, defined as

$$\mathrm{He} = f\frac{L}{c} \tag{16}$$

in which c is the average speed of sound in the plenum and the combustion chamber weighted by their relative length, f is the dominant frequency, and L is the total length of the combustor

$$\mathrm{St} = f\frac{h}{u} \tag{17}$$

in which f is the dominant frequency, u is the characteristic speed of the upstream cold flow, and h is the characteristics length of the bluff body.

If the dominant frequency is driven by the acoustics of the system, the Helmholtz number remains constant as the Reynolds number of the incoming flow changes, while the Strouhal number

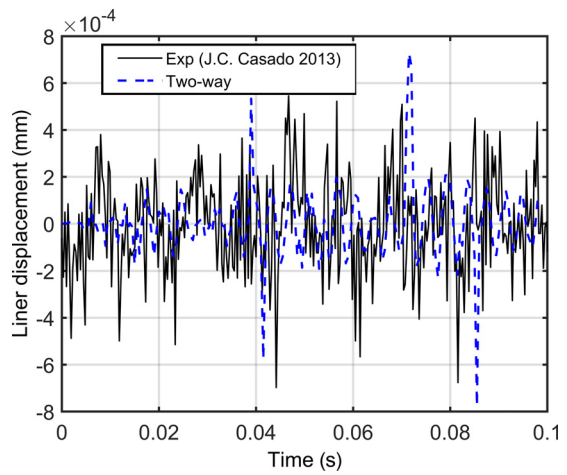

Fig. 12: Two-way FSI (dash line) and experimental (solid line) results for the wall displacement of the case 40 kW and $\lambda = 1.4$

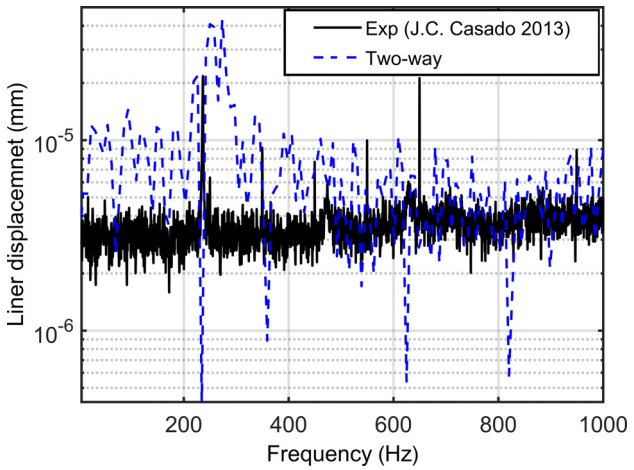

Fig. 13 Wall displacement results obtained from the two-way FSI approach (dash line) and experimental data (solid line) versus the frequency for the case 40 kW and $\lambda = 1.4$

varies hyperbolically. The recorded Helmholtz and Strouhal numbers at the observed dominant frequencies, shown in Fig. 11 for different Reynolds numbers, confirm that the LCO is driven by the acoustics of the LIMOUSINE combustor as the Helmholtz number stays almost constant at an approximate value of 0.4.

5.2 Structural Behavior. Figure 12 shows the calculated and measured wall displacement at a location of 200 mm downstream the burner. The time domain indicates a wall displacement in order of 100 μm from the not loaded position. Figure 13 shows the measured and calculated liner displacement frequency spectra; one can see that the peaks present in the pressure spectrum are approximately reproduced in the wall displacement results. This indicates a strong fluid–structure interaction around the natural modes of the combustor. In the experiment, frequencies of 237 Hz and 474 originate from the gas phase flame dynamics. In the numerical data, the main instability peak is observed approximately at 250 Hz, which is close to the first experimental value of 237 Hz. However, because the physical time for the computation of the two-way numerical calculations is limited, the pressure plots have low frequency resolution. The peaks observed at 550 Hz and 650 Hz are coming from the structural dynamics. These oscillations are fed by energy derived from the acoustic fluid oscillation but vibrate at the structural eigenfrequencies. As it was mentioned before, due to the existence of the temperature gradient along the chamber and therefore variable material properties as a function of temperature, the structural frequencies observed in the pressure and displacement spectra deviate from the presented values in Table 2. In the experiment, the instability peak at 650 is as strong as the one observed at 237 Hz, which is not the case in the simulation.

6 Conclusion

Thermoacoustic instability can be caused by the feedback mechanism between unsteady heat release, acoustic oscillations, and flow perturbations. In a gas turbine combustor, limit cycles of pressure oscillations at elevated temperatures generated by the

unstable combustion process enhance the structural vibration levels of the combustor. Depending on the operating conditions, the flame may show a stable or an unstable behavior. In order to predict the frequency and magnitude of the thermoacoustic instabilities, and also to capture the reacting flow physics coupled to the structure, calculations are performed for an unstable flame condition. To model the flame dynamics, CFD approach is used, while FEM code is used to determine the dynamic response of a structure under unsteady pressure loads. These two solvers are coupled using partitioned approach. The transient information (pressure and displacement) is exchanged between the fluid and structural domain by means of two-way coupling. The obtained results using this approach were compared with zero-way interaction model as well as the CHT approach. The main outcome of this research is summarized as follows:

- Among the used models, the zero-way interaction model results show the largest discrepancy from experimental results in the prediction of instability frequencies.
- The frequencies of the thermoacoustic instabilities are well predicted using the CHT and two-way coupled approaches, while in the latter case the magnitude is slightly overpredicted; this can be explained by overprediction of the temperature in the CFD domain due to the assumed constant temperature at the structure. While in the CHT modeling results, due to the modeling of the transient heat transfer and therefore considering the correct heat losses from the system, the predicted pressure field is closer to the experiments.
- Although the CHT approach gives very accurate information of the characteristics frequencies and amplitude, to determine the influence of the LCO behavior on the structure and/or the effect of structural vibrations on the confined fluid in the unstable regime, a two-way coupled FSI model is required.
- The preliminary results of solid deformation show that the maximal displacement exhibited by the structure is very small, a fraction of a millimeter. Such displacements are extremely small but can act like a strong acoustic source due to the high acceleration rate of the structure.

Funding Data

- EC in the Marie Curie Actions Networks for Initial Training, under call FP7-PEOPLE-2007-1-1-ITN, Project LIMOUSINE (Project No. 214905).

References

[1] Lieuwen, T., Torres, H., Johnson, C., and Zinn, B. T., 2000, "A Mechanism of Combustion Instability in Lean Premixed Gas Turbine Combustors," ASME J. Eng. Gas Turbines Power, **123**(1), pp. 182–189.

[2] Huang, Y., and Yang, V., 2009, "Dynamics and Stability of Lean-Premixed Swirl-Stabilized Combustion," Prog. Energy Combust. Sci., **35**(4), pp. 293–364.

[3] Altunlu, A. C., van der Hoogt, P. J. M., and de Boer, A., 2014, "Sensitivity of Combustion Driven Structural Dynamics and Damage to Thermo-Acoustic Instability: Combustion-Acoustics-Vibration," ASME J. Eng. Gas Turbines Power, **136**(5), p. 051501.

[4] Dowling, A. P., 1995, "The Calculation of Thermoacoustic Oscillations," J. Sound Vib., **180**(4), pp. 557–581.

[5] Huls, R., 2006, "Acousto-Elastic Interaction in Combustion Chambers," Ph.D. dissertation, University of Twente, Enschede, The Netherlands.

[6] Ahn, K., and Yu, K. H., 2012, "Effects of Damköhler Number on Vortex–Flame Interaction," Combust. Flame, **159**(2), pp. 686–696.

[7] Xie, G., Zhang, W., and Sunden, B., 2012, "Computational Analysis of the Influences of Guide Ribs/Vanes on Enhanced Heat Transfer of a Turbine Blade Tip-Wall," Int. J. Therm. Sci., **51**, pp. 184–194.

[8] Kim, K. M., Park, J. S., Lee, D. H., Lee, T. W., and Cho, H. H., 2011, "Analysis of Conjugated Heat Transfer, Stress and Failure in a Gas Turbine Blade With Circular Cooling Passages," Eng. Failure Anal., **18**(4), pp. 1212–1222.

[9] Huls, R. A., Sengissen, A. X., van der Hoogt, P. J. M., Kok, J. B. W., Poinsot, T., and de Boer, A., 2007, "Vibration Prediction in Combustion Chambers by Coupling Finite Elements and Large Eddy Simulations," J. Sound Vib., **304**(1–2), pp. 224–229.

[10] Pozarlik, A. K., and Kok, J. B. W., 2014, "Fluid-Structure Interaction in Combustion System of a Gas Turbine—Effect of Liner Vibrations," ASME J. Eng. Gas Turbines Power, **136**(9), p. 091502.

[11] Petchenko, A., Bychkov, V., Akkerman, V. Y., and Eriksson, L.-E., 2007, "Flame–Sound Interaction in Tubes With Nonslip Walls," Combust. Flame, **149**(4), pp. 418–434.

[12] Foucher, F., Burnel, S., Mounaïm-Rousselle, C., Boukhalfa, M., Renou, B., and Trinité, M., 2003, "Flame Wall Interaction: Effect of Stretch," Exp. Therm. Fluid Sci., **27**(4), pp. 431–437.

[13] Lefebvre, A. H., and Ballal, D. R., 2010, *Gas Turbine Combustion: Alternative Fuels and Emissions*, Taylor & Francis, Abington, UK.

[14] Candel, S., 2002, "Combustion Dynamics and Control: Progress and Challenges," Proc. Combust. Inst., **29**(1), pp. 1–28.

[15] Leppington, F. G., 1978, "Acoustic Scattering by Membranes and Plates With Line Constraints," J. Sound Vib., **58**(3), pp. 319–332.

[16] Shen, H., Wen, J., Yu, D., Asgari, M., and Wen, X., 2013, "Control of Sound and Vibration of Fluid-Filled Cylindrical Shells Via Periodic Design and Active Control," J. Sound Vib., **332**(18), pp. 4193–4209.

[17] Schotté, J. S., and Ohayon, R., 2013, "Linearized Formulation for Fluid–Structure Interaction: Application to the Linear Dynamic Response of a Pressurized Elastic Structure Containing a Fluid With a Free Surface," J. Sound Vib., **332**(10), pp. 2396–2414.

[18] Pozarlik, A. K., 2010, "Vibro-Acoustical Instabilities Induced by Combustion Dynamics in Gas Turbine Combustors," Ph.D. dissertation, University of Twente, Enschede, The Netherlands.

[19] Alemela, P., Casado, J., Kumar, S., and Kok, J., 2013, "Thermoacoustic Analysis of the Dynamic Pressure Inside a Model Combustor During Limit Cycle Oscillations," Int. J. Spray Combust. Dyn., **5**(1), pp. 25–48.

[20] Altunlu, A. C, Shahi, M., Pozarlik, A. K., van der Hoogt, P. J. M., Kok, J. B. W., and de Boer, A., 2012, "Fluid-Structure Interaction on the Combustion Instability," 19th International Congress on Sound and Vibration (ICSV), Vilnius, Lithuania, July 8–12, pp. 291–298.

[21] Bothien, M. R., Moeck, J. P., and Oliver Paschereit, C., 2008, "Active Control of the Acoustic Boundary Conditions of Combustion Test Rigs," J. Sound Vib., **318**(4–5), pp. 678–701.

[22] Rayleigh, J., 1878, "The Explanation of Certain Acoustical Phenomena," Nature, **18**(455), pp. 319–321.

[23] Nicoud, F., and Poinsot, T., 2005, "Thermoacoustic Instabilities: Should the Rayleigh Criterion Be Extended to Include Entropy Changes?," Combust. Flame, **142**(1–2), pp. 153–159.

[24] Polifke, W., Poncet, A., Paschereit, C. O., and Döbbeling, K., 2001, "Reconstruction of Acoustic Transfer Matrices by Instationary Computational Fluid Dynamics," J. Sound Vib., **245**(3), pp. 483–510.

[25] Rijke, P. L., 1859, "On the Vibration of the Air in a Tube Open at Both Ends," Philos. Mag., **17**(116), pp. 419–422.

[26] Maity, D., and Bhattacharyya, S. K., 2003, "A Parametric Study on Fluid–Structure Interaction Problems," J. Sound Vib., **263**(4), pp. 917–935.

[27] Michler, C., Hulshoff, S. J., van Brummelen, E. H., and de Borst, R., 2004, "A Monolithic Approach to Fluid–Structure Interaction," Comput. Fluids, **33**(5–6), pp. 839–848.

[28] Blom, F. J., 1998, "A Monolithical Fluid-Structure Interaction Algorithm Applied to the Piston Problem," Comput. Methods Appl. Mech. Eng., **167**(3–4), pp. 369–391.

[29] Felippa, C. A., Park, K. C., and Farhat, C., 2001, "Partitioned Analysis of Coupled Mechanical Systems," Comput. Methods Appl. Mech. Eng., **190**(24–25), pp. 3247–3270.

[30] Piperno, S., Farhat, C., and Larrouturou, B., 1995, "Partitioned Procedures for the Transient Solution of Coupled Aeroelastic Problems—Part I: Model Problem, Theory and Two-Dimensional Application," Comput. Methods Appl. Mech. Eng., **124**(1–2), pp. 79–112.

[31] Piperno, S., and Farhat, C., 2001, "Partitioned Procedures for the Transient Solution of Coupled Aeroelastic Problems—Part II: Energy Transfer Analysis and Three-Dimensional Applications," Comput. Methods Appl. Mech. Eng., **190**(24–25), pp. 3147–3170.

[32] Hübner, B., Walhorn, E., and Dinkler, D., 2004, "A Monolithic Approach to Fluid–Structure Interaction Using Space–Time Finite Elements," Comput. Methods Appl. Mech. Eng., **193**(23–26), pp. 2087–2104.

[33] Storti, M. A., Nigro, N. M., Paz, R. R., and Dalcín, L. D., 2009, "Strong Coupling Strategy for Fluid–Structure Interaction Problems in Supersonic Regime Via Fixed Point Iteration," J. Sound Vib., **320**(4–5), pp. 859–877.

[34] Schäfer, M., Heck, M., and Yigit, S., 2006, "An Implicit Partitioned Method for the Numerical Simulation of Fluid-Structure Interaction," *Fluid-Structure Interaction*, H.-J. Bungartz, and M. Schäfer, eds., Springer, Berlin, pp. 171–194.

[35] Gatzhammer, B., 2008, "A Partitioned Approach for Fluid-Structure Interaction on Cartesian Grids," Master's thesis, Technische Universität München, Munich, Germany.

[36] Gövert, S., and Kok, J. B. W., 2013, "Fluid-Structure Coupling for Numerical Simulations of a Gas Turbine Combustor," 20th International Congress on Sound and Vibration, Bangkok, Thailand, July 7–11, pp. 2986–2994.

[37] Shahi, M., Kok, J. B. W., Pozarlik, A., Roman Casado, J. C., and Sponfeldner, T., 2013, "Sensitivity of the Numerical Prediction of Turbulent Combustion Dynamics in the LIMOUSINE Combustor," ASME J. Eng. Gas Turbines Power, **136**(2), p. 021504.

[38] Patankar, S. V., 1980, *Numerical Heat Transfer and Fluid Flow*, Hemisphere, New York.

[39] Kumar, T. V. S., Alemela, P. R., and Kok, J. B. W., 2011, "Dynamics of Flame Stabilized by Triangular Bluff Body in Partially Premixed Methane-Air Combustion," ASME Paper No. GT2011-46241.

[40] Forkel, H., 2012, "CFX 14.5 Burning Velocity Model Discretization for Non-Premixed Combustion," ANSYS Inc., Canonsburg, PA.

[41] Smooke, M. D., Puri, I. K., and Seshadri, K., 1988, "A Comparison Between Numerical Calculations and Experimental Measurements of the Structure of a Counterflow Diffusion Flame Burning Diluted Methane in Diluted Air," Symp. (Int.) Combust., **21**(1), pp. 1783–1792.
[42] ANSYS, 2011, "ANSYS CFX Solver Manager User's Guide, Release 14.0," ANSYS Inc., Canonsburg, PA.
[43] Altunlu, A. C., 2013, "The Analysis of Mechanical Integrity in Gas Turbine Engines Subjected to Combustion Instabilities," Ph.D. dissertation, University of Twente, Enschede, The Netherlands, p. 182.
[44] Blevins, R. D., 1984, *Formulas for Natural Frequency and Mode Shape*, Krieger Publishing, Malabar, FL.
[45] ANSYS, 2011, "ANSYS Mechanical APDL Element Reference, Release 14.0," ANSYS Inc., Canonsburg, PA.
[46] Shahi, M., Kok, J. B. W., Casado, J. C. R., and Pozarlik, A., 2014, "Assessment of Thermoacoustic Instabilities in a Partially Premixed Model Combustor Using URANS Approach," Appl. Therm. Eng., **71**(1), pp. 276–290.
[47] Filosa, A., Shahi, M., Tomasello, A., Noll, B., Aigner, M., and Kok, J., 2013, "Numerical Studies of Unsteady Heat Transfer With Thermoacoustics Oscillations," 20th International Congress on Sound and Vibration, Bangkok, Thailand, July 7–11, pp. 3018–3026.
[48] Roman Casado, J. C., 2013, "Nonlinear Behavior of the Thermoacoustic Instabilities in the Limousine Combustor," Ph.D. dissertation, University of Twente, Enschede, The Netherlands.
[49] Sivakumar, R., and Chakravarthy, S. R., 2008, "Experimental Investigation of the Acoustic Field in a Bluff-Body Combustor," Int. J. Aeroacoustics, **7**(3–4), pp. 267–299.